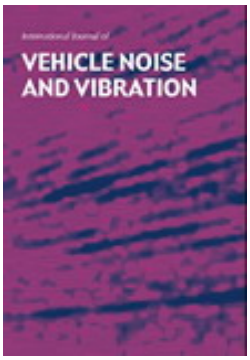

International Journal of Vehicle Noise and Vibration

ISSN online: 1479-148X - ISSN print: 1479-1471
https://www.inderscience.com/ijvnv

Virtual wind tunnel modelling and numerical calculation of forklift power compartment based on acoustic-heat-flow multi-physical field coupling

Enlai Zhang, Jingjing Zhang, Jiahe Lin

DOI: 10.1504/IJVNV.2023.10055200

Article History:
Received: 21 December 2019
Accepted: 04 May 2021
Published online: 10 April 2023

Virtual wind tunnel modelling and numerical calculation of forklift power compartment based on acoustic-heat-flow multi-physical field coupling

Enlai Zhang

School of Mechanical and Automotive Engineering,
Xiamen University of Technology,
Xiamen, 361024, China
and
College of Chengyi University,
Jimei University,
Xiamen, 361021, China
Email: zhangenlai1986@163.com

Jingjing Zhang*

College of Applied Science and Technology,
Hainan University,
Danzhou, 571737, China
Email: 993958@hainanu.edu.cn
*Corresponding author

Jiahe Lin

Department of Mechanical and Electrical Engineering,
Xiamen University,
Xiamen, 361005, China
Email: 719285248@qq.com

Abstract: Considering the contradiction between increasing heat flow density and noise decibel decreasing requirement in forklift power compartment, this paper theoretically analyses the multi-physical field coupling relationship between the sound, heat and flow velocity fields in the non-ideal medium. For the acoustic radiation problem in infinite domain, the perfectly matched layer (PML) boundary is introduced, and a virtual wind tunnel model is established based on finite element method and boundary element method (FEM-BEM). Finally, the sound pressure and temperature distributions of the forklift power compartment are obtained by numerical simulation, and then the calculation accuracy of the established virtual wind tunnel model is verified by tests.

Keywords: forklift power compartment; virtual wind tunnel model; PML; perfectly matched layer; FEM-BEM; finite element method and boundary element method.

Reference to this paper should be made as follows: Zhang, E., Zhang, J. and Lin, J. (2023) 'Virtual wind tunnel modelling and numerical calculation of forklift power compartment based on acoustic-heat-flow multi-physical field coupling', *Int. J. Vehicle Noise and Vibration*, Vol. 19, Nos. 1/2, pp.1–14.

Biographical notes: Enlai Zhang is an Associate Professor, graduated from Xiamen University for PhD and completed Postdoctoral Research in Xiamen King Long United Automotive Industry Co., Ltd. His main research interests are vehicle noise reduction and sound quality optimisation. He has presided over a number of scientific and technological projects supported by National Natural Science Foundation of China, China Postdoctoral Science Foundation, Natural Science Foundation of Fujian Province and so on. At present, he has published some SCI/EI academic papers in authoritative journals such as *Applied Acoustics*.

Jingjing Zhang is the Vice Dean of School of Applied Science and Technology, Hainan University, and Director of Department of Internet of Things Engineering. He has published seven academic articles in SCI and presided over many projects such as the Natural Science Foundation of Hainan Province. His main research directions are signal analysis and processing, sensor and internet of things system.

Jiahe Lin graduated from the Department of Mechanical and Electrical Engineering in Xiamen University with a Master's degree. His research directions are vehicle noise, vibration and harshness (NVH). During his study, he participated in a number of national and enterprise research projects and published several authoritative papers.

1 Introduction

Noise reduction and sound quality have been important aspects of vehicle NVH research (Nopiah et al., 2015; Zhang et al., 2016; Zhang et al., 2018). However, for high-power engineering vehicles, along with a large number of thermal dense flow and radiation noise increases, it is necessary to seek a balance between noise reduction and thermal management. Generally, sound propagation is not only related to the type of medium and the speed, but also to temperature. The acoustic wave radiated from the structure surface in vehicle power compartment is affected by the temperature and air velocity to some extent. Multiple physical fields involved in vehicle running mainly include structure field, sound field, heat field and flow velocity field. Among them, the vibration structure field and the radiated sound field are uncoupled, due to obtaining the structural response first through the measurement, and then calculating the acoustic response directly from the structural response (Shi et al., 2018). However, with the increase of the vehicle engine power and the heat flow density in power compartment, the noise radiated by the whole vehicle becomes larger, which leads to the contradiction between the increasing heat flow and the decreasing noise requirement. Therefore, it is particularly important to establish a virtual wind tunnel model of acoustic radiation, heat transfer and air flow with mutual influence, and to conduct numerical research.

In practice, finite element method (FEM) and boundary element method (BEM) are generally combined to solve the vibration and acoustic problems, giving full play to their advantages (Duan et al., 2021; Li et al., 2017; Gao et al., 2018; Lock and Holloway, 2016): FEM is suitable for complex geometrical shape, and BEM can solve the acoustic radiation problems in infinite domain. Using the numerical method of FEM-BEM, the Helmholtz equation of the structure surface and sound radiation from engineering vehicle can be derived, and the particle velocity and sound pressure in the medium are directly

obtained through the structural vibration acceleration. In recent years, computational fluid dynamics (CFD) has been widely applied to the heat transfer simulation in medium (Zhao et al., 2020; Goktepeli et al., 2020; Ngo and Phu, 2020). For example, Liu et al. (2014) carried out numerical analysis of three improved schemes for radiators in a virtual wind tunnel using CFD, and studied the heat dissipation performance of each scheme. Zhang et al. (2016) used the virtual wind tunnel and numerical simulation to predict the impact of exhaust systems on the thermal environment in vehicle power compartment, and compared heat exchange efficiencies under two exhaust system structures. Their research results provided a guidance for the heat management simulation.

It is not difficult to find that the existing numerical studies separate the cooling and heat dissipation in vehicle power compartment from the structural acoustic radiation, but the acoustic radiation and the heat dissipation in air medium may interact with each other to a certain extent. Therefore, this paper presents the multi-field coupling analysis, modelling and numerical calculation for the acoustic-heat-flow field in forklift power compartment.

2 Structural acoustic radiation

The sound source can be approximately calculated by structural surface particles under the continuity condition between normal vibration acceleration and sound pressure. The governing equation of sound pressure and normal acceleration from structural acoustic radiation is expressed as follows

$$-\boldsymbol{n}\cdot\left(-\frac{1}{\rho}(\nabla p-q)\right)=\boldsymbol{a}_{\boldsymbol{n}} \tag{1}$$

where $\boldsymbol{n}$ is the unit normal vector pointed outside the solid domain; ρ is the density; p is the sound pressure; q is a dipole source; $\boldsymbol{a}_{\boldsymbol{n}}$ is the initial acceleration of structural surface vibration; ∇ is the divergence operator. Therefore, after obtaining the vibration acceleration of the power compartment structure surface, the main noise sources can be set. In addition, the walls of other structures are hard sound field boundary conditions. The hard boundary can be simulated using hard sound field boundary condition with the normal acceleration of zero.

As we all know, in free space, the sound waves generated by structures propagate directly to the atmosphere without reflection, but this process cannot be solved by finite element modelling alone. It is necessary to deal with the acoustic radiation boundary with absorption cutoff in order to simulate the non-reflection phenomenon. The perfectly matched layer (PML) is an effective way to solve this problem (Arslan et al., 2017; Assi and Cobbold, 2016).

PML is an analogue technique for rapidly attenuating the incident wave at the boundary, which is suitable for any incidence angle. Figure 1 shows a schematic diagram of the PML area, where 0 is the boundary node; the area smaller than 0 is the calculation area, that is, the finite field; and the area greater than 0 is the PML area. The incident wave is attenuated exponentially from the finite area into the PML area, and in theory, the larger the PML area, the more obvious the attenuation of incident waves.

Figure 1 Domain transformation of finite element and PML (see online version for colours)

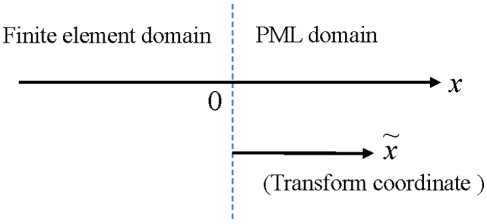

One-dimensional boundary equation is introduced to understand PML theory, and the frequency domain expression of one-dimensional acoustic wave equation is described as

$$-\omega^2 u = V^2 \frac{\partial^2 u}{\partial x^2} \tag{2}$$

where u is the displacement; V is the speed, and ω is the angular frequency.

According to calculus, the solution form of equation (2) is $A\exp[i(\omega t - kx)]$, where A is the amplitude and k is the number of internal waves of 2π length. PML method is used to make solution expression as $A\exp[i(\omega t - kx - \gamma(x))]$ When in the PML region, $\gamma(x) > 0$, and with the increase of x, the wave decays along the x direction by exponential function to ensure that the reflection coefficient between the finite field and PML boundary is close to zero.

A common decay function $d(x)$ was proposed by Festa and Nielsen (2003), and its mathematical is expressed as

$$d(x) = \begin{cases} 0 & x < 0 \\ \log\left(\dfrac{1}{R}\right)\dfrac{(n+1)\sqrt{\dfrac{\mu_R}{\rho}}}{2\delta}\left(\dfrac{x}{\delta}\right)^n & x \geq 0 \end{cases} \tag{3}$$

where δ is the thickness of PML region; R is a reflection coefficient, generally $R = 10^{-3}$. When $n = 2$ and $x \geq 0$, $d(x)$ represents the damping function. The advantage of this attenuation function has been verified by the related studies (Duru and Kreiss, 2014).

3 Heat transfer

When the power compartment works, structural surface temperature gradually increases, and the high temperature area transfers heat to the low temperature area, while structural surface temperature can continuously exchange heat with the flowing air in contact, thus causing the heat convection in the flowing air (Liu et al., 2020). In general, the third boundary condition of heat transfer can be used when the object surface is engaged in heat convection or radiation dissipation with the air. The following governing equation describes the fluid-solid heat transfer process.

$$\rho C_p \mathbf{u} \cdot \nabla T = \nabla \cdot (k \nabla T) + Q_1 - Q_p \tag{4}$$

In the formula, ρ is fluid density; C_p is the specific heat capacity under constant pressure; T represents the absolute temperature; $\mathbf{u}$ is a flow velocity vector; k is a material heat conductivity; Q_1 and Q_p stand for heat source and heat loss item, respectively.

4 Multi-physical field coupling in acoustic-heat-flow

Equation (1) indicates that the acoustic pressure divergence is related to fluid density, and equation (4) describes that the fluid-solid heat transfer is affected by structural surface temperature and flow velocity. Therefore, the coupling relationship between sound field, heat field and flow field in non-ideal medium can be explored through structural sound pressure, medium density, flow velocity and heat conduction (Cramer, 2012; Liu et al., 2021). In equation (4), the Q_p refers to the heat loss caused by structural wall viscosity and heat conduction in a non-ideal medium. It is necessary to introduce the heat loss effect in the medium and structural cladding layer loss into the control equations. Usually, viscous fluid motion involves the following equations.

$$\rho \frac{d\mathbf{u}}{dt} = \nabla \cdot \boldsymbol{\sigma} \tag{5}$$

$$\frac{d\rho}{dt} + \rho(\nabla \cdot \mathbf{u}) = 0 \tag{6}$$

$$\rho C_p \frac{dT}{dt} - \alpha_0 T \frac{dp}{dt} = -\nabla \cdot (-k\nabla T) + \phi(\mu, \mu_B, \mathbf{u}) + Q \tag{7}$$

$$\boldsymbol{\sigma} = -p\boldsymbol{I} + \boldsymbol{\tau} = -p\boldsymbol{I} + \mu(\nabla \mathbf{u} + (\nabla \mathbf{u})^T) - \left(\frac{2\mu}{3} - \mu_B\right)(\nabla \cdot \mathbf{u})\boldsymbol{I} \tag{8}$$

As can be seen from the above equations, the control variables are sound pressure p, flow rate $\mathbf{u}$, temperature T and fluid density ρ. In the above formulas, μ is the dynamic viscosity coefficient; μ_B is a volume viscosity coefficient; α_0 is the thermal expansion coefficient in constant pressure, and $\boldsymbol{I}$ represents the strength vector. Furthermore, equation (5) is the momentum equation, namely Navier-Stokes (N-S); equation (6) is the continuous equation; equation (7) is the energy expression based on Fourier heat conduction law, and equation (8) describes the constitutive relationship between total stress tensor $\boldsymbol{\sigma}$ and viscous stress tensor $\boldsymbol{\tau}$.

In the energy equation, the viscous dissipation equation is expressed as a function of viscous stress tensor $\boldsymbol{\tau}$ and tensor rate S:

$$\phi = \boldsymbol{\tau}(\mathbf{u}) : S(\mathbf{u}) \tag{9}$$

where both of two tensors are functions of the velocity vector, and the symbol of ':' refers to the second derivative operator.

In the time domain, in order to make the above equations (5)–(7) conform to the steady-state medium dissipation after Fourier transform, and combine with the constitutive equation to establish the coupling relationship in the time domain, the incremental equation is required to have the ability of matching the time-harmonic solution. For the steady-state solution of harmonic oscillation, the independent source terms and variables can be assumed as:

$$\mathbf{u} = \mathbf{u}_0 + \mathbf{u}'e^{i\omega t};\quad p = p_0 + p'e^{i\omega t};\quad T = T_0 + T'e^{i\omega t};\quad \rho = \rho_0 + \rho'e^{i\omega t};\quad Q = Q_0 + Q'e^{i\omega t} \tag{10}$$

For the initial static system environment, it is easy to know $\mathbf{u}_0 = 0$, and substitute equations (8)–(10) into equations (5)–(7) to obtain the functional expressions between sound pressure p, temperature T and flow velocity $\mathbf{u}$:

$$i\omega\rho_0\mathbf{u} = \nabla\cdot\left(-p\boldsymbol{I} + \mu(\nabla\mathbf{u} + (\nabla\mathbf{u})^T - \left(\frac{2\mu}{3} - \mu_B\right)(\nabla\cdot\mathbf{u})\boldsymbol{I}\right) \tag{11}$$

$$i\omega\rho + \rho_0(\nabla\cdot\mathbf{u}) = 0 \tag{12}$$

$$i\omega\rho_0 C_P T = -\nabla\cdot(-k\nabla T) + i\omega p T_0\alpha_0 + Q \tag{13}$$

To some extent, the above equations realise the coupling relationship between the acoustic, thermal and flow fields in a non-ideal viscous and dissipative media.

5 Virtual wind tunnel modelling and numerical calculation

The above theoretical analysis requires virtual wind tunnel modelling and numerical calculation with the help of the multi-physical field coupling COMSOL platform (Jiang et al., 2016; Sangare et al., 2016). Because the internal structures in forklift power compartment are very complex, in order to improve the accuracy and efficiency of numerical calculation, simplify and clean some physical models before meshing, remove the geometric parts not affecting the analysis results, mainly including oil pipes, small round holes, pin shaft, chamfer, etc., and the retained geometric model dimensions should be consistent with the actual sizes. The simplified 3D physical model is shown in Figure 2.

Figure 2 3D solid model of the simplified forklift power compartment (see online version for colours)

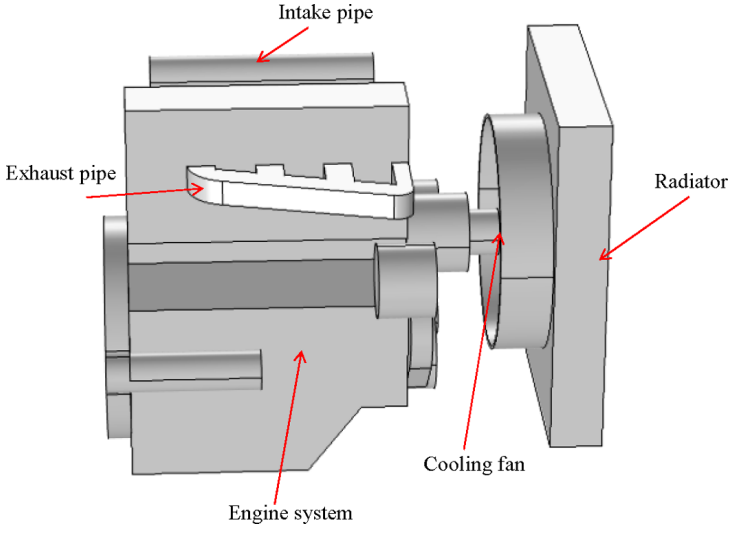

Since the multi-physical field coupling of the power compartment involves the sound, temperature and flow fields, it is necessary to establish an air domain outside the solid domain to calculate the physical field distribution in the air. At the same time, the PML of three-dimensional sphere was introduced to simulate the computational domain of cut-off acoustic radiation. Finally, the virtual wind tunnel physical and mesh models of the forklift power compartment were established, as shown in Figure 3.

In the COMSOL platform, the boundary conditions mainly include: structural vibration and sound radiation in the cut-off calculation domain, fluid flow model, solid heat source and gas-solid convection heat transfer, fan boundary and porous media model, etc. The specific settings are shown in Figure 4.

Figure 3 Virtual wind tunnel models based on PML, (a) physical model and (b) mesh model

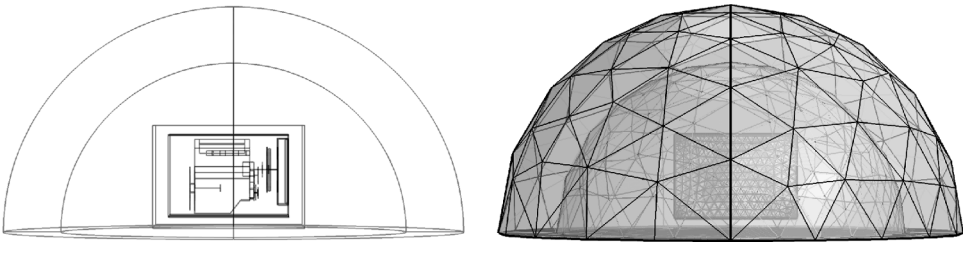

(a) (b)

Figure 4 Boundary conditions for multi-physical field coupling modelling (see online version for colours)

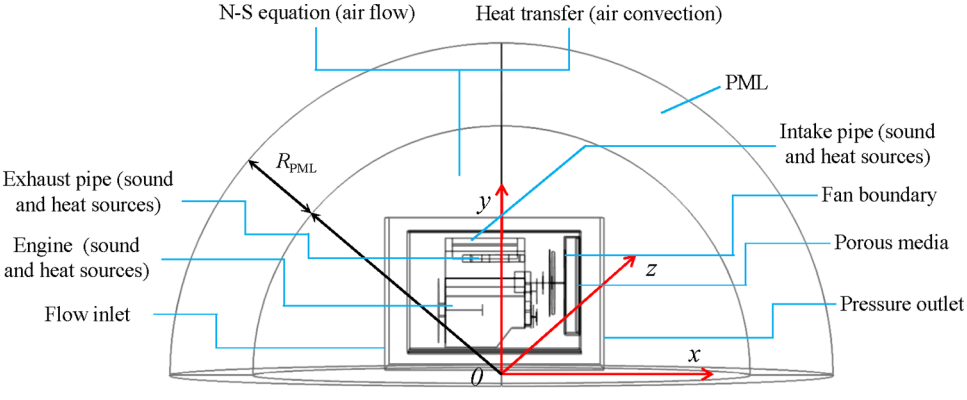

5.1 Acoustic radiation simulation

In order to obtain vibration accelerations from structure surfaces in the forklift power compartment, the vibration tests at idle speed were carried out using acceleration sensors and the Zonicbook 618/E digital acquisition system.

Based on the previous noise source identification results, 8 measuring points of the test prototype engine system were selected, respectively arranged at the upper and lower ends of engine suspension, engine surfaces, exhaust and intake pipes (Zhang et al., 2015). The data analysis results showed that the central frequency from engine surfaces, exhaust and intake pipes reached the maximum vibration acceleration near 2,000 Hz, 1,600 Hz

and 800 Hz, corresponding to 1.45 m/s^2, 2.51 m/s^2 and 1.226 m/s^2, respectively. These accelerations were input in the COMSOL by selecting the corresponding structural surfaces to set as noise sources. Furthermore, add that the thickness of the PML boundary layer in this acoustic radiation simulation was set to $R_{\mathrm{PML}} = 0.5$ m.

5.2 Turbulence simulation

In the engineering application, the average N-S equation is usually applied to describe the three-dimensional irregular turbulent motion, and the k-ε turbulence model is commonly used, that is, the turbulent kinetic energy equation of k is expressed as follows

$$\rho(\mathbf{u}\cdot\nabla)k = \nabla\cdot\left[\left(\mu+\frac{\mu_T}{\sigma_k}\right)\nabla k\right] + P_k - \rho\varepsilon \tag{14}$$

The dissipation rate equation of ε for turbulent kinetic energy is described as

$$\rho(\mathbf{u}\cdot\nabla)\varepsilon = \nabla\cdot\left[\left(\mu+\frac{\mu_T}{\sigma_\varepsilon}\right)\nabla\varepsilon\right] + C_{\varepsilon 1}\frac{\varepsilon}{k}P_k - C_{\varepsilon 2}\rho\frac{\varepsilon^2}{k} \tag{15}$$

where μ is the dynamic viscosity, and turbulent dynamic viscosity is $\mu_T = \rho C_\mu \frac{k^2}{\varepsilon}$, $p_k = \mu_T\left[\nabla \mathrm{u} : \left(\nabla \mathrm{u} + (\nabla \mathrm{u})^T\right)\right]$; σ_k and σ_ε stand for the turbulent Prandtl numbers of k and ε, respectively, which represents relative values of heat diffusion and momentum in the fluid.

In this simulation case, the turbulence model parameters are taken as $C_{\varepsilon 1} = 1.44$; $C_{\varepsilon 2} = 1.92$; $C_\mu = 0.09$; $\sigma_k = 1$; $\sigma_\varepsilon = 1.3$.

5.3 Heat transfer simulation

The temperature change of the structural vibration body in the non-ideal medium satisfies the third kind of boundary condition of heat conduction, that is to say, the system structure surface temperature is set to realise the gradient change of temperature in the normal direction, which can be expressed by the following equation.

$$-k\frac{\partial T}{\partial n}\Big|_{\Gamma 3} = h(T_{ext} - T) \tag{16}$$

where h and T_{ext} are convective heat transfer coefficient and external ambient temperature, respectively, and $\Gamma 3$ represents the third type of boundary condition.

After the forklift power compartment was in stable operation, the surface temperatures of the engine body, exhaust pipe, radiator and intake pipe were obtained by a infrared thermometer as 75°C, 102°C, 41°C and 56°C, respectively, and the corresponding surface temperatures were set in the COMSOL platform.

5.4 Fan boundary simulation

In the actual simulation, the fan operation can be described using the flow boundary condition of any flow speed, the main boundary parameters are static pressure and flow rate, and the governing equation can be expressed as

$$p - \mathbf{n}^T \left[\mu(\nabla \mathbf{u}) + (\nabla \mathbf{u})^T \right] \mathbf{n} + \rho(\mathbf{u} \cdot \mathbf{n})^2 = \Delta p \tag{17}$$

The fan data about static pressure and flow rate were measured and provided by the manufacturer according to the standard of GB/T1236-2000, as shown in Table 1. Similarly, these parameters were also set at the fan boundaries in the COMSOL platform.

Table 1 Relationship between flow rate and static pressure at different rotating speeds

Rotating speed (r/min)	2,500	3,000	3,500	4,000
Flow rate (m^3/s)	1.01	1.22	1.41	1.62
Static pressure (Pa)	193.2	277.9	372.8	481.3

5.5 Radiator simulation

Due to the small gap between the heat exchanger tube and the radiator fin and complex structure, it is difficult to directly perform the finite element modelling for the radiator. But using a porous medium model is an effective way to handle the radiator simulation (Lee et al., 2014; Mao et al., 2010). For porous materials with hard skeleton, the famous Delany-Bazley model estimates the material impedance parameters as a function about frequency and flow resistance rate, and the basic coefficients of Delany-Bazley are shown as

$$k_c = k_a \cdot \left(1 + 0.098 \cdot \left(\frac{\rho_a f}{R_f} \right)^{-0.7} - i \cdot 0.189 \cdot \left(\frac{\rho_a f}{R_f} \right)^{-0.595} \right) \tag{18}$$

$$Z_c = Z_a \cdot \left(1 + 0.057 \cdot \left(\frac{\rho_a f}{R_f} \right)^{0.734} - i \cdot 0.087 \cdot \left(\frac{\rho_a f}{R_f} \right)^{-0.732} \right) \tag{19}$$

In the formula, k_c and Z_c are complex wave number and impedance respectively, R_f represents fluid impedance, and $k_a = \omega/c_a$ and $Z_a = \rho_a c_a$ are free space wave number and air impedance, respectively. The porous acoustic model is a preset selection of the Delany-Bazley-Miki model under porous domain characteristics in the COMSOL platform, in which the flow resistance comes from the material with a porosity of 0.62.

5.6 Numerical calculation and verification

Based on the above virtual wind tunnel modelling and boundary condition analysis, define global parameters, import geometric model, define PML; add 'pressure acoustics, frequency domain' module, 'internal normal acceleration' and 'internal hard sound field' to simulate structural sound radiation; add 'solid heat transfer' module, 'fluid heat transfer', 'porous medium heat transfer', 'Turbulent k-ε', 'internal fan' to simulate heat

transfer. The acoustic radiation and temperature distribution at different frequencies were obtained, and Figure 5 shows the total acoustic pressure distribution in the power compartment at a frequency of 60 Hz, and Figure 6 indicates the corresponding temperature distribution inside the power compartment.

Figure 5 Distribution of total sound pressure field in power compartment (Pa, f = 60 Hz); three different views, (a) global contour, (b) top contour and (c) main contour (see online version for colours)

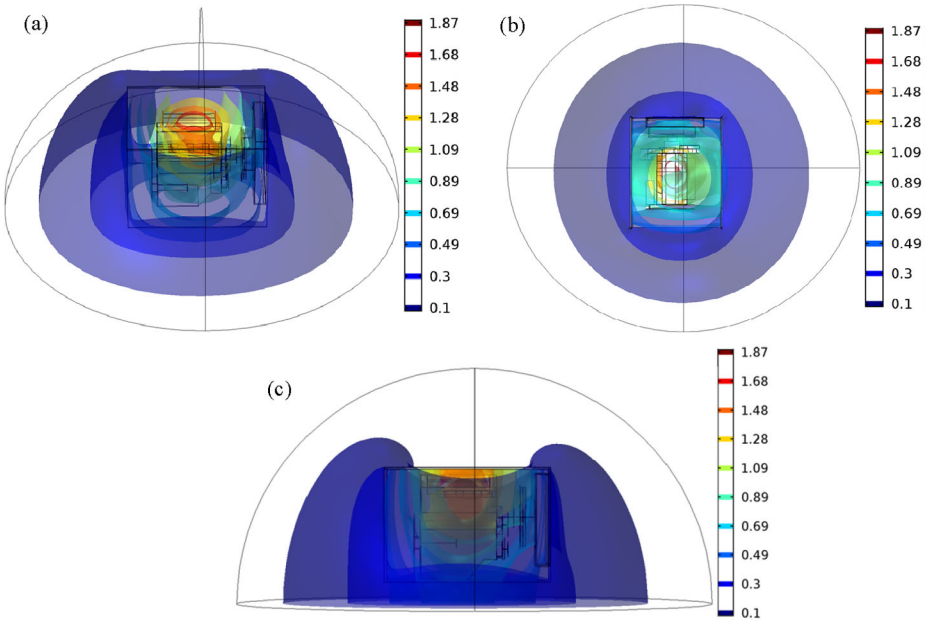

As can be found from Figure 5(a), the maximum sound pressure is mainly concentrated in the engine system of the power compartment and radiates sound waves outward from it as the main sound source. Meanwhile, because the actual bottom of the power compartment is open, the sound source radiates sound pressure directly to the bottom, left and right sides [see Figure 5(c)], and forms evenly distributed sound pressure equivalent surface.

The following phenomena can be seen from Figure 6: Temperature is radiated from the left to the right direction of the radiator, because the whole forklift adopts exhaust cooling form, and the structural temperature generated during the system operation is convective heat transfer with the surrounding air, and performs forced convection in the power compartment under the cooling fan drive, thus taking structural surface temperature and conducting thermal radiation along the flow direction, which is consistent with the actual heat dissipation characteristics of the power compartment. The heat is concentrated near the exhaust pipe and engine surface, similarly the actual power compartment bottom is open, and a portion of the heat radiates heat outward through the bottom [see Figure 6(d)].

Figure 6 Temperature field distribution: (a) global contour; (b) top contour; (c) global section and (d) top section (see online version for colours)

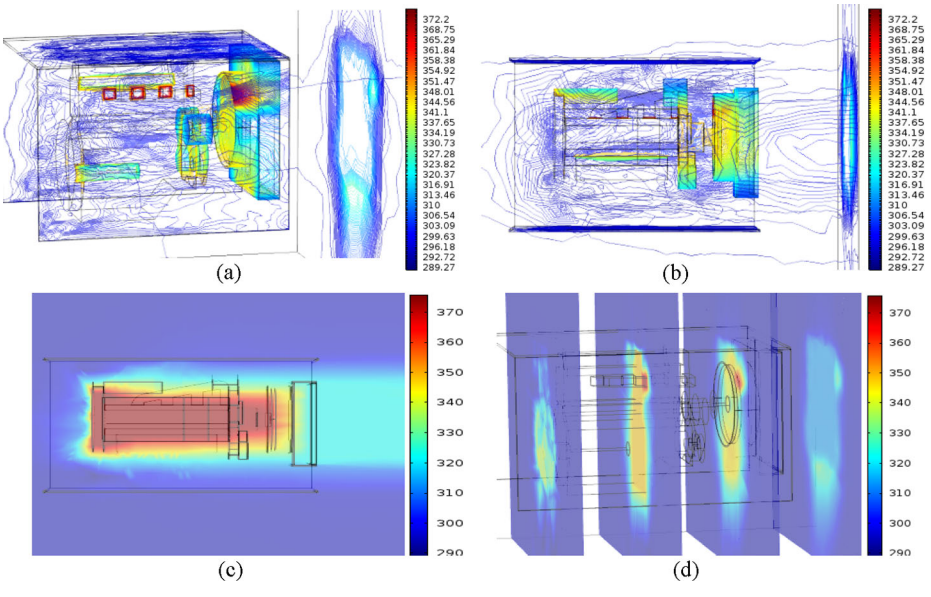

In order to verify the numerical calculation accuracy of multi-physical field coupling modelling, the sound pressure level of the radiated noise outside the power compartment and the internal temperature were compared. The noise observation points were 1 m from the horizontal and vertical axis of the prototype centre to the outer structure surface, and noise test instrument of HS5633 was adopted for testing. In addition, the temperature measurement points distributed in the power compartment were on the left, right and top centre of the horizontal and vertical axis, as shown in Figure 7(a), and thermocouple sensors and data recorder were WRKK-103 and LR8400-21, respectively.

Figure 7 Temperature measuring equipment: (a) thermocouple sensor and (b) data recorder (see online version for colours)

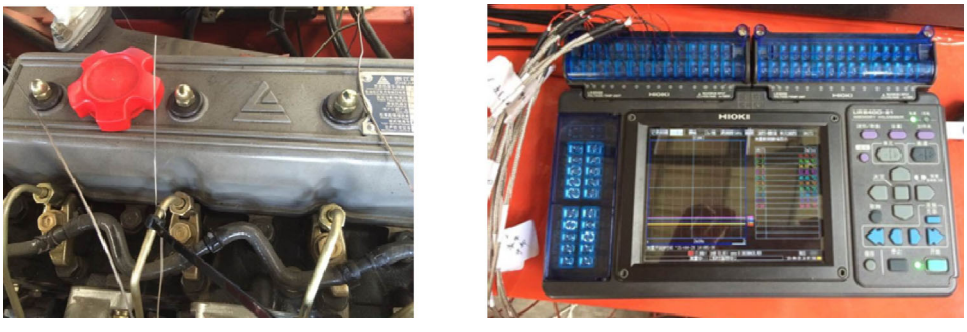

(a) (b)

In the virtual wind tunnel model created by COMSOL, the sound pressure level and temperature calculated by numerical simulation can be obtained by selecting points of derived values, and then compared with the test data. The comparison results show that

the average relative errors between the calculated radiated sound pressure level and internal temperature and the experimental values are 4.54% and 6.76% respectively within the allowable ranges, which verifies the numerical calculation accuracy of the virtual wind tunnel model based on multi-physical field coupling.

6 Conclusions

Noise control requirements are increasingly strict, but engineering vehicles gradually develop to the high power direction, resulting in the constantly increasing heat flow density and noise decibel, which is a thorny problem faced by current engineering vehicles. To solve this problem, a numerical calculation scheme based on multi-physical field coupling analysis is proposed in this paper. Firstly, the control method of acoustic radiation propagation from vibration structures in the medium and fluid-solid heat transfer are analysed, and the PML is introduced to solve the acoustic no-reflection problem at the cut-off boundary; Secondly, the coupling relationships of the sound, temperature and flow velocity fields in the non-ideal medium are theoretically analysed, and taking the forklift power compartment as the research object, a virtual wind tunnel model is established to realise the numerical calculation of multi-physical field coupling in the COMSOL platform. This process includes establishing physical and grid models, setting up sound sources and heat sources based on experimental data, simulating acoustic radiation, turbulence, heat transfer, fan boundaries and radiator porous media, etc. Finally, the accuracy of the virtual wind tunnel model calculation with multi-physical field coupling is verified through experiments, which can lay an important technical foundation for the energy saving and acoustic optimisation in the next work.

Acknowledgements

The work was supported by Xiamen Youth Innovation Foundation (3502Z20206024), Science and Technology Project for High-level Talents (YKJ22017R) and Key Project of Research and Development in Hainan Province (ZDYF2020038).

References

Arslan, E., Ozyoruk, Y. and Caliskan, M. (2017) 'Numerical analysis of one-dimensional sound propagation through a duct containing water droplets', *Journal of Computational Acoustics*, Vol. 25, No. 1, p.1650017.

Assi, H. and Cobbold, R.S.C. (2016) 'A perfectly matched layer formulation for modeling transient wave propagation in an unbounded fluid-solid medium', *Journal of the Acoustics Society of America*, Vol. 139, No. 4, pp.1528–1536.

Cramer, M.S. (2012) 'Numerical estimate for the bulk viscosity of ideal gases', *Physics of Fluids*, Vol. 24, No. 6, p.066102.

Duan, J.X., Zhang, L., Sun, X.H., Chen, W.J. and Da, L.L. (2021) 'An equivalent source CVIS method and its application in predicting structural vibration and acoustic radiation in ocean acoustic channe', *Ocean Engineering*, Vol. 222, p.108570.

Duru, K. and Kreiss, G. (2014) 'Efficient and stable perfectly matched layer for CEM', *Applied Numerical Mathematics*, Vol. 76, pp.34–47.

Festa, G. and Nielsen, S. (2003) 'PML absorbing boundaries', *Bulletin of the Seismological Society and America*, Vol. 93, No. 2, pp.891–903.

Gao, R.X., Zhang, Y.H. and Kennedy, D. (2018) 'A hybrid boundary element-statistical energy analysis for the mid-frequency vibration of vibro-acoustic systems', *Computers & Structures*, Vol. 203, pp.34–42.

Goktepeli, L., Atmaca, U. and Cakan, A. (2020) 'Investigation of heat transfer augmentation between the ribbed plates via Taguchi approach and computational fluid dynamics', *Journal of Thermal Science*, Vol. 29, No. 3, pp.647–666.

Jiang, G.S., Liu, Y.C., Kong, Q., Xu, W.L. and An, L.S. (2016) 'The sound transmission through tube arrays in power boilers based on phononic crystals theory', *Applied Thermal Engineering*, Vol. 99, pp.1133–1140.

Lee, S.H., Hur, N. and Kang, S. (2014) 'An efficient method to predict the heat transfer performance of a louver fin radiator in an automotive power system', *Journal of Mechanical Science and Technology*, Vol. 28, No. 1, pp.145–155.

Li, P.B., Yan, Y.J. and Lin, H.G. (2017) 'Numerical simulation and experimental researches on the vibration-acoustic coupled property of an aircraft model under strong reverberation noise', *Journal of Vibration and Control*, Vol. 23, No. 17, pp.2757–2766.

Liu, C.C., Liu, Z.C., Tian, J., Xu, Y., Yang, Z.Y. and Wang, P.H. (2020) 'Investigations of energy, exergy distribution characteristics of overall working conditions and effect of key boundary parameters on residual energy availability in an automotive turbocharged diesel engine', *Applied Thermal Engineering*, Vol. 174, p.115352.

Liu, J.X., Qin, S.C., Xu, Z.Y., Zhang, A., Xi, X. and Zhang, X.L. (2014) 'Improvement and analysis of heat exchange performance of vehicle radiator module in virtual tunnel', *Jilin Daxue Xuebao (Gongxueban)*, Vol.44, No. 2, pp.330–334, DOI: 10.13229/ j.cnki.jdxbgxb201402009.

Liu, Y.Y., Rao, Y., Yang, L., Xu, Y.M. and Terzis, A. (2021) 'Flow and heat transfer characteristics of double-wall cooling with multi-row short film cooling hole arrangements', *International Journal of Thermal Sciences*, Vol. 165, p.106878.

Lock, A. and Holloway, D. (2016) 'Boundary element modelling of a novel simple enhanced bandwidth schroeder diffuser offering comparable performance to a fractal design', *Acoustics Australia*, Vol. 44, No. 1, pp.137–147.

Mao, S.L., Cheng, C.R. and Li, X.C. (2010) 'Michaelides EE. Thermal/structural analysis of radiators for heavy-duty trucks', *Applied Thermal Engineering*, Vol. 30, Nos. 11–12, pp.1438–1446.

Ngo, T.T. and Phu, N.M. (2020) 'Computational fluid dynamics analysis of the heat transfer and pressure drop of solar air heater with conic-curve profile ribs', *Journal of Thermal Analysis and Calorimetry*, Vol. 139, No. 5, pp.3235–3246.

Nopiah, Z.M., Junoh, A.K. and Ariffin, A.K. (2015) 'K-means clustering and neural network for evaluating sound level vibration in vehicle cabin', *Journal of Vibration and Control*, Vol. 21, No. 9, pp.1698–1720.

Sangare, D., Bostyn, S., Moscosa-Santillan, M. and Gokalp, L. (2016) 'Hydrodynamics, heat transfer and kinetics reaction of CFD modeling of a batch stirred reactor under hydrothermal carbonization conditions', *Energy*, Vol. 219, p.119635.

Shi, S.X., Su, Z., Jin, G.Y. and Liu, Z.G. (2018) 'Vibro-acoustic modeling and analysis of a coupled acoustic system comprising a partially opened cavity coupled with a flexible plate', *Mechanical Systems and Signal Processing*, Vol. 98, pp.324–343.

Zhang, E.L., Hou, L. and Yang, W.P. (2015) 'Noise source identification and experimental research of engine compartment of a forklift based on fast independent component analysis and Scan & Paint', *Proceedings of The ASME 2015 International Mechanical Engineering Congress & Exposition*, 13–19 November, p.V013T16A022, Houston, Texas.

Zhang, E.L., Hou, L., Shen, C., Shi, Y.L. and Zhang, Y.X. (2016) 'Sound quality prediction of vehicle interior noise and mathematical modeling using aback propagation neural network (BPNN) based on particle swarm optimization (PSO)', *Measurement Science and Technology*, Vol. 27, No. 1, p.015801.

Zhang, E.L., Zhang Q.M., Xiao, J.J., Hou, L. and Guo, T. (2018) 'Acoustic comfort evaluation modeling and improvement test of a forklift based on rank score comparison and multiple linear regression', *Applied Acoustics*, Vol. 135, pp.29–36.

Zhang, Q.G., Qin, S.C., Yang, L.G., Ma, R.D., Liu, Y.F. and Liu, W. (2016) 'Thermal environment prediction of loader engine cabin in a virtual tunnel', *Jilin Daxue Xuebao (Gongxuebao)*, Vol. 46, No. 1, pp.50–56, DOI: 10.13229/j.cnki.jdxbgxb2016010080

Zhao, P., Xu, J., Liu, X.C., Ge, W. and Wang, J.W. (2020) 'A computational fluid dynamics – discrete element-immersed boundary method for Cartesian grid simulation of heat transfer in compressible gas-solid flow with complex geometries', *Physics of Fluids*, Vol. 32, No. 10, p.103306.